Hindawi
Mathematical Problems in Engineering
Volume 2022, Article ID 6888916, 12 pages
https://doi.org/10.1155/2022/6888916

Research Article

Long-Term Bearing Deformation Characteristics of Caved Gangue in Gob under Different Moisture Conditions

Zhen Wang,[1] Shanming Wei,[2] Zhenhua Zhao,[2,3] Liting Xing,[4] Changsuo Li,[2,3] and Hailong Wang[2,3,5]

[1]*Lixia Holding Group Co. LTD, Jinan 250000, China*
[2]*No. 801 Hydrogeology and Engineering Geological Brigade of Shandong Provincial Bureau of Geology and Mineral Resources, Jinan 250014, China*
[3]*Shandong Provincial Bureau of Geology and Mineral Resources, Jinan 250013, China*
[4]*School of Water Conservancy and Environment, University of Jinan, Jinan 250022, China*
[5]*School of Civil Engineering and Architecture, Linyi University, Linyi 276000, China*

Correspondence should be addressed to Shanming Wei; 95526734@qq.com and Hailong Wang; whlmlp@163.com

Received 4 March 2022; Accepted 26 March 2022; Published 15 April 2022

Academic Editor: Fuqiang Ren

In gob, the caved gangue is in a state of long-term bearing deformation with obvious time-dependent effect, even though the coal seam has been mined for a long time. As time goes on, because of the excessive deformation of caved gangue, the gob surrounding rock will easily aggravate the structural instability and cause dynamic disasters, such as mine water inrush and surface collapse. If the gob is filled with water, the bearing capacity of the caved gangue in waterlogged environment will be worse than that in dry environment, which will greatly increase the possibility of disasters. In order to study the bearing deformation characteristics of caved gangue under different moisture conditions, a testing system used for bearing deformation testing of caved gangue is developed. The typical caved gangue is chosen for samples. In view of the particle size distribution characteristics and stress state of caved gangue, the size distribution of caved gangue obeys the law of normal distribution and the load pattern is designed to step load. With the increase of axial load, the axial deformation of caved gangue increases gradually, the residual bulking coefficient decreases gradually, which are more obvious in load stage than in constant load stage. In the early constant load stage, the axial deformation of caved gangue grows rapidly, then tends to be slow and steady gradually; the relationship between strain and time meets the logarithmic relationship. In load stage, the D-value of axial strain decreases gradually along with the increase of axial load, whereas in constant load stage, it is opposite; the bearing deformation of caved gangue is consisted of two parts: instantaneous compression deformation and long-term deformation. For instantaneous compression deformation, the water acting as the lubricant promotes the compressive strain of caved gangue specimen and is conducive to rotation and slipping between each rock block. For long-term deformation, meanwhile, the water acting as the softening agent reduces the strength of the rock block and is conducive to the crushing of the rock block. The newborn rock blocks may slip and fill the gap between rock blocks, which also promotes the compressive strain of caved gangue specimen. The research results have important significance for forecasting and controlling the movement and deformation of overlying strata caused by mining.

1. Introduction

There are three distinct zones (caved zone, fracture zone, and continuous deformation zone) of disturbance in overlying strata when the coal seam roof is controlled by caving method, based on the deformation and failure characteristics of overlying strata [1–7]. The caved zone is filled by the caved gangue composed of an immediate roof and part overlying strata [8, 9], as shown in Figure 1. The vertical height of the caved zone with a highly irregular shape and different granular caved gangue can reach 4–11 times the mining height [10, 11]. The caved gangue is gradually compressed by the overburden load resulting from mining disturbance, which supports the deformable upper rock strata [12, 13].

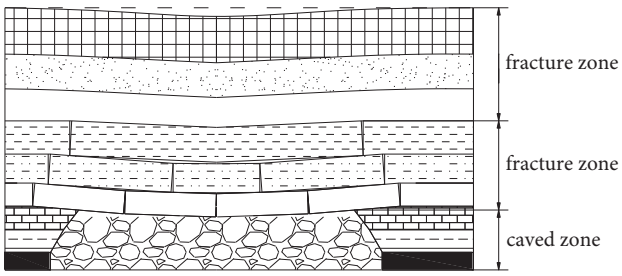

Figure 1: Overlying strata failure mode after mining.

Therefore, the variable load compaction of caved gangue in gob directly determines the movement of the upper strata.

The caved gangue in gob can be treated as a porous medium consisting of caved gangue blocks generated by caving, pilling, and recompressing [14]. Due to the nonuniform stress distribution in a gob, the degree of compaction of caved gangue mass varies with location and time, resulting in a variable load compaction. It is well known that the mining-induced gob stress profile near the working face region varies with the mining direction [15–17], as shown in Figure 2. Apparently, the gob close to the working face has a relatively low-stress situation due to the existence of hydraulic supports and the overburden hinge structure. Moving away from the working face towards the gob, the load carried by the caved gangue gradually increases, which results in a progressive compaction of the loosely packed rocks. The stress level of the caved zone far away from the working face almost recovers back to the original in-situ value and the gob was fully compacted. The caved gangue is in a state of long-term bearing deformation with obvious time-dependent effect, even though the coal seam has been mined for a long time. As time goes on, because of the excessive deformation of caved gangue in gob, the gob surrounding rock will easily aggravate the structural instability and cause dynamic disasters, such as mine water inrush and surface collapse [18–20]. If the gob is filled with water, the bearing capacity of the caved gangue in waterlogged environment will be worse than that in dry environment, which will greatly increase the possibility of disasters. Thus, it is essential to study the bearing deformation characteristics of caved gangue in gob under load, especially with different moisture contents. The results are difficult to obtain by field observation. Because of the concealment of underground excavation engineering, laboratory testing becomes an effective way to solve this problem [21–33].

In the process of laboratory testing, the bearing deformation characteristics of caved gangue are mainly influenced by the own characteristics of specimens and the properties of experimental device. The own characteristics of specimen include compressive strength, particle size, particle size distribution, and moisture content. The properties of experimental device include the size of test vessel, load method, and measuring accuracy. Based on partial influencing factor, some scholars have carried out a series of studies on the caved gangue [34–39]. These studies significantly contribute to the understanding of bearing deformation characteristics of caved gangue. However, the small effective volume of the existing experimental devices is the common defect. With the increase of particle size of caved gangue, the problem of boundary effect will become more and more prominent. Moreover, the patterns of particle size distribution of caved gangue are varied, and the existing studies are mainly focused on single particle size distribution, uniform particle size distribution, and continuous particle size distribution. In this study, in order to study the bearing deformation characteristics of large-size caved gangue, a testing system used for bearing deformation testing of large-size caved gangue was developed. The typical sandstone from the roof was chosen for specimens. In view of the particle size distribution characteristics and stress state of caved gangue in caved zone, the size distribution of caved gangue obeyed the law of normal distribution, and the load method was designed to step load. The research results have important significance for forecasting and controlling the movement and deformation of overlying strata caused by mining.

2. Testing System and Scheme

2.1. Testing System. The testing system used for bearing deformation testing of large-size caved gangue is consisted of load support bracket, load head, testing chamber, servo control system of displacement and load, servo control system of water pressure and water yield, and operating deck, as shown in Figure 3. (1) Load support bracket is consisted of base, frame, supporting structure of hydraulic cylinder, reaction frame, which plays the role of fixed, and supporting action. (2) Load head is connected to hydrocylinder by connecting rod. (3) Testing chamber is cylindric, the effective size are 400 mm diameter and 680 mm high. In order to facilitate the filling of caved gangue specimens, the testing chamber is composed of two compartments. (4) Servo control system of displacement and stress can control the load head by setting displacement or load. The meter full scale of displacement is 400 mm, and the accuracy is 0.01 mm. The maximum load is 600 KN, and the accuracy is 0.01 KN. (5) Servo control system of water pressure and water yield can fill the testing chamber with water by setting water pressure or water yield. The maximum water pressure is 2 MPa, the maximum water supply is 150 L/h, and the accuracy is 0.01 MPa. (6) Operating deck is fully automated, five basic parameters can be collected into a database in real time, such as time, displacement, load, water pressure, and water yield. The maximum sampling frequency is 10HZ.

2.2. Testing Scheme

2.2.1. Particle Size Distribution. The rock specimens are sandstone from the gob of Daizhuang coal mine, which is located near Jining city, Shandong Province, China. Some basic parameters are shown in Table 1. Considering the scale effect, the ratio between the diameter of caved gangue specimen and the maximum particle size of caved gangue should be greater than or equal to 5 [40–42]. Because the internal diameter of testing chamber is 400 mm, the

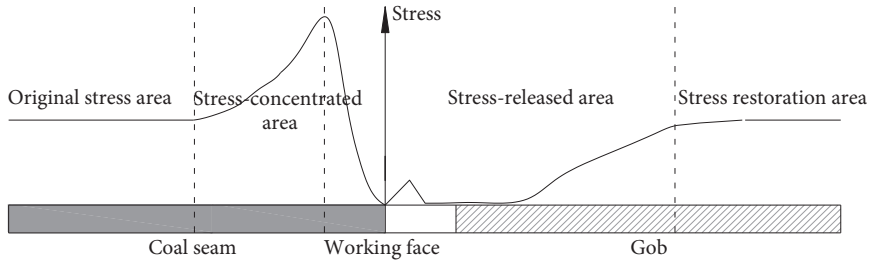

Figure 2: Stress distribution around gob.

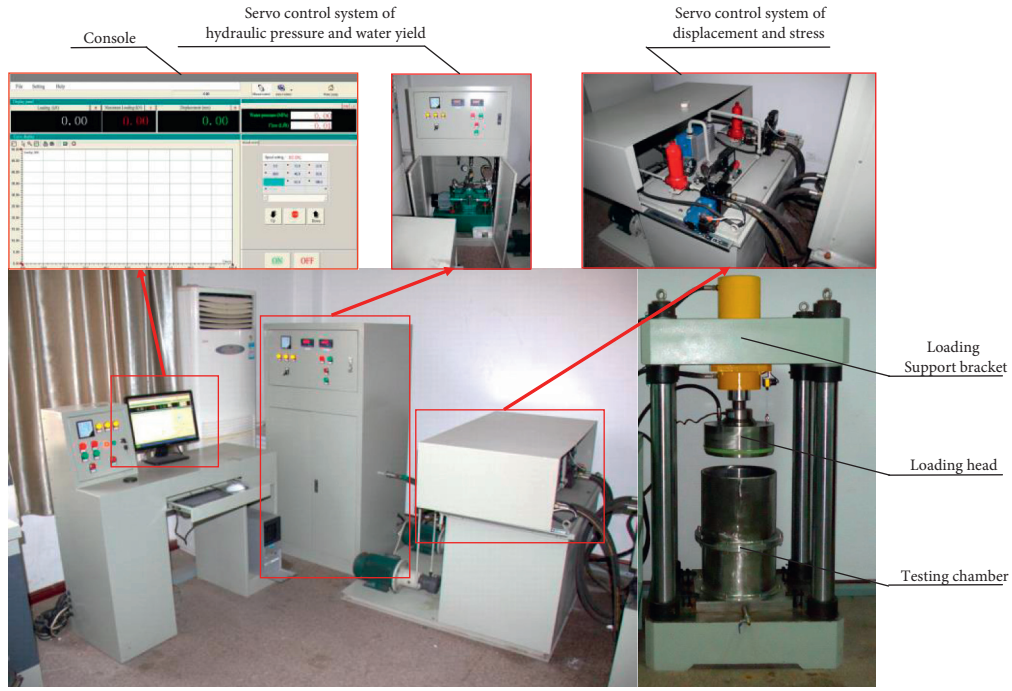

Figure 3: Testing system used for bearing deformation testing of large-size caved gangue.

Table 1: Basic parameters of sandstone.

Moisture condition	Uniaxial compressive strength (MPa)	Tensile strength (MPa)	Modulus of elasticity (GPa)	Poisson's ratio	Density (kg/m^3)	Moisture content (%)
Dry	96.78	7.5	16.1	0.199	2565.6	0
Water saturated	87.21	7.2	15.2	0.209	2578.8	0.516

maximum particle size of caved gangue could be tested is 80 mm. In order to minimize the influence of size effect on the testing results, the maximum particle size of the caved gangue selected in the test is determined to be 40 mm. The caved gangue is divided into 7 categories by the particle size, which are 5–10 mm, 10–15 mm, 15–20 mm, 20–25 mm, 25–30 mm, 30–35 mm, and 35~40 mm, as shown in Figure 4. In this article, the size distribution of caved gangue specimens for testing obeys the law of normal distribution. In a complete caved gangue specimen, according to the particle size of caved gangue from small to large, the mass fraction of 7 categories is 5%, 10%, 20%, 30%, 20%, 10%, and 5%, respectively, as shown in Figure 5. For the caved gangue with a certain particle size, the relation between the mass fraction and particle size is as follows:

$$A = 4.885 + \frac{329.279}{10.761\sqrt{\pi/2}} e^{-2(D-2)^2/10.761^2}, \quad (1)$$

where A is the mass fraction of the caved gangue with a certain particle size (%) and D is the minimum of the caved gangue in a certain particle size (mm).

The actual height of caved gangue specimen is 655 mm, and the total mass is 110 kg. The initial bulking factor of caved gangue specimen is 1.901, and the voidage is 0.901. The assembled caved gangue specimen is shown in Figure 6.

The initial bulking factor of caved gangue (K) is given by

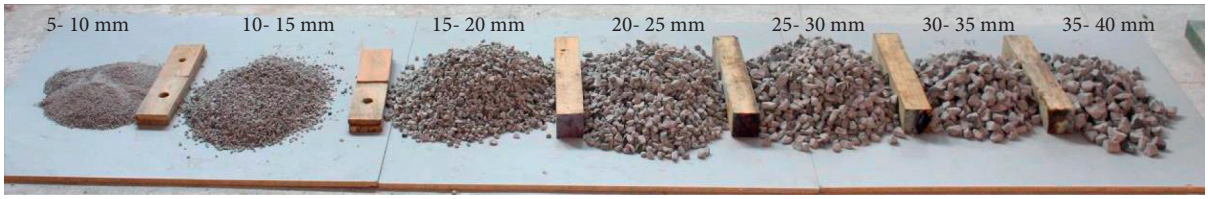

Figure 4: Caved gangue with different particle sizes.

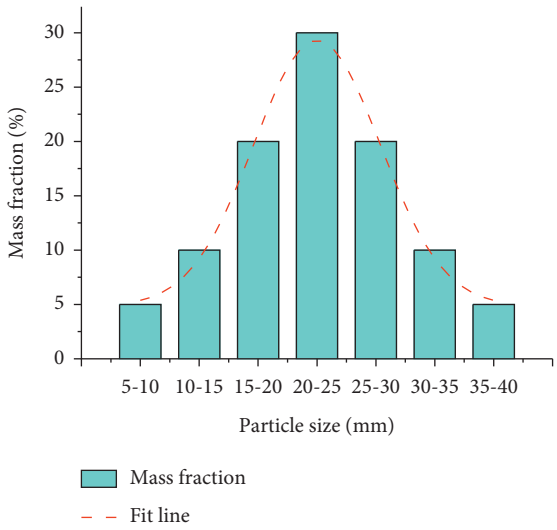

Figure 5: Mass fraction of 7 categories of caved gangue.

$$K = \frac{V_1}{V_0}, \tag{2}$$

where K is the initial bulking factor of caved gangue, V_0 is the volume of complete rock, and V_1 is the volume of caved gangue produced by complete rock in the state of natural accumulation.

The initial voidage of caved gangue (P) is given by

$$P = \frac{V_1 - V_0}{V_0} = K - 1, \tag{3}$$

where P is the initial voidage of caved gangue.

The residual height of caved gangue specimen after the bearing deformation testing (h_1) is given by

$$h_1 = h_0 - u, \tag{4}$$

where h_1 is the residual height of caved gangue specimen after the bearing deformation testing (mm), h_0 is the initial height of caved gangue specimen (mm), and u is the deformation of caved gangue specimen (mm).

The residual bulking factor of caved gangue specimen after the bearing deformation testing (K_1) is given by

$$K_1 = \frac{h_1 \cdot S}{V_0}, \tag{5}$$

where K_1 is the residual bulking factor of caved gangue specimen after the bearing deformation testing and S is the area of testing chamber, 125600 mm^2.

Figure 6: Assembled caved gangue.

2.2.2. Load Method. The pressure acting on the caved gangue in gob is mainly from overlying strata. The pressure value is directly related to the height of the fractured overlying strata and increases with the increase in the height of the fractured overlying strata. In the time interval of two adjacent roof weightings, the pressure acting on the caved gangue in gob is basically unchanged, which is equal to the self-weight stress of total fractured overlying strata. During the roof weighting, the pressure acting on the caved gangue in gob will increase rapidly, and the increment is equal to the self-weight stress of generated fractured overlying strata. So the pressure acting on the caved gangue in gob is stair stepping, which provides evidence for designing the load method in the bearing deformation testing of caved gangue in gob. The load method is divided into 2 stages, namely, load stage and constant load stage. In load stage, the load speed is 0.5 kN/s. In constant load stage, the constant load is 100 kN, 200 kN, 300 kN, and 400 kN, respectively; the duration of each constant load is 4 hours. Before the formal testing, a preload of 20 kN is applied to the caved gangue in gob specimen until the deformation is constant, which needs about 15 minutes. The load method of a complete testing is shown as Figure 7.

3. Testing Results and Analysis

3.1. Bulking and Deformation Characteristics. The parameters of caved gangue specimens during different testing stage are shown in Table 2. With the increase of axial load, the axial deformation of caved gangue specimen increases gradually, as shown in Figure 8(a). The final deformation of caved gangue specimen under dry condition and water-saturated condition is 74.07 mm and 91.00 mm, respectively, and the corresponding strain value is 113.1×10–3 and 138.9×10–3, respectively. The residual bulking factor of

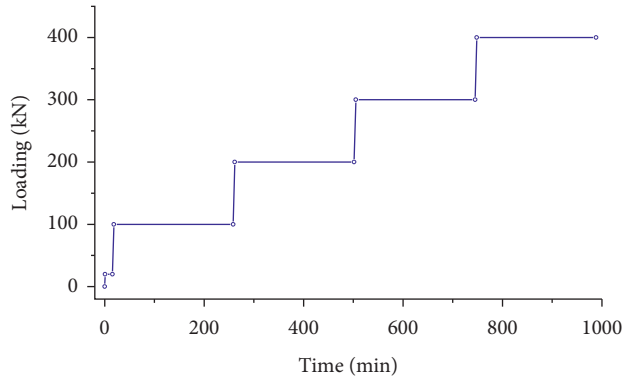

Figure 7: Load method of a complete testing.

Table 2: Parameters of caved gangue specimens during different testing stage.

Moisture condition	Testing stage	Deformation			Strain			Residual bulking factor	
		Initial value (mm)	Final value (mm)	D-value (mm)	Accumulated strain/10^{-3}	Fitting formula of strain-time	R-square	Initial value	Final value
Dry	20–100 kN load	0	20.82	20.82	31.8	—	—	1.901	1.840
	100 kN constant load	20.82	23.01	2.19	35.1	$\varepsilon = 33.77 + 0.25 \ln t$	0.982	1.840	1.834
	100–200 kN load	23.01	38.38	15.37	58.6	—	—	1.834	1.789
	200 kN constant load	38.38	42.23	3.85	64.5	$\varepsilon = 59.72 + 0.85 \ln t$	0.970	1.789	1.778
	200–300 kN load	42.23	54.47	12.24	83.2	—	—	1.778	1.743
	300 kN constant load	54.47	59.67	5.20	91.1	$\varepsilon = 86.37 + 0.91 \ln t$	0.973	1.743	1.727
	300–400 kN load	59.67	68.88	9.21	105.2	—	—	1.727	1.701
	400 kN constant load	68.88	74.07	5.19	113.1	$\varepsilon = 109.90 + 0.59 \ln t$	0.941	1.701	1.686
Water Saturated	20–100 kN load	0	21.27	21.27	32.5	—	—	1.901	1.839
	100 kN constant load	21.27	25.30	4.03	38.6	$\varepsilon = 34.24 + 0.80 \ln t$	0.996	1.839	1.827
	100–200 kN load	25.30	45.10	19.80	68.9	—	—	1.827	1.770
	200 kN constant load	45.10	53.19	8.09	81.2	$\varepsilon = 71.64 + 1.75 \ln t$	0.995	1.770	1.746
	200–300 kN load	53.19	64.26	11.07	98.1	—	—	1.746	1.714
	300 kN constant load	64.26	72.61	8.35	110.9	$\varepsilon = 101.66 + 1.69 \ln t$	0.995	1.714	1.690
	300–400 kN load	72.61	81.75	9.14	124.8	—	—	1.690	1.663
	400 kN constant load	81.75	91.00	9.25	138.9	$\varepsilon = 128.63 + 1.92 \ln t$	0.994	1.663	1.637

Notes: ε is the accumulated strain of caved gangue specimen, $\times 10^{-3}$, t is the hold time in each constant load stage, min.

caved gangue specimen under dry condition and water-saturated condition decreases gradually, which changes from 1.901 to 1.686 and from 1.901 to 1.637, respectively, as shown in Figure 8(b). The axial deformation in load stage is more obvious than that in constant load stage, which accounts for 77.8% of total deformation under dry condition and 67.6% of total deformation under water-saturated condition. The testing results indicate that the water promotes the compressive strain of caved gangue specimen obviously.

In order to show the change of the axial deformation of the caved gangue specimens in constant load stage intuitively, the axial strain-time curves are made, as shown in Figure 9. The fitting formulas of strain-time curves in different constant load stages are shown in Table 2. The

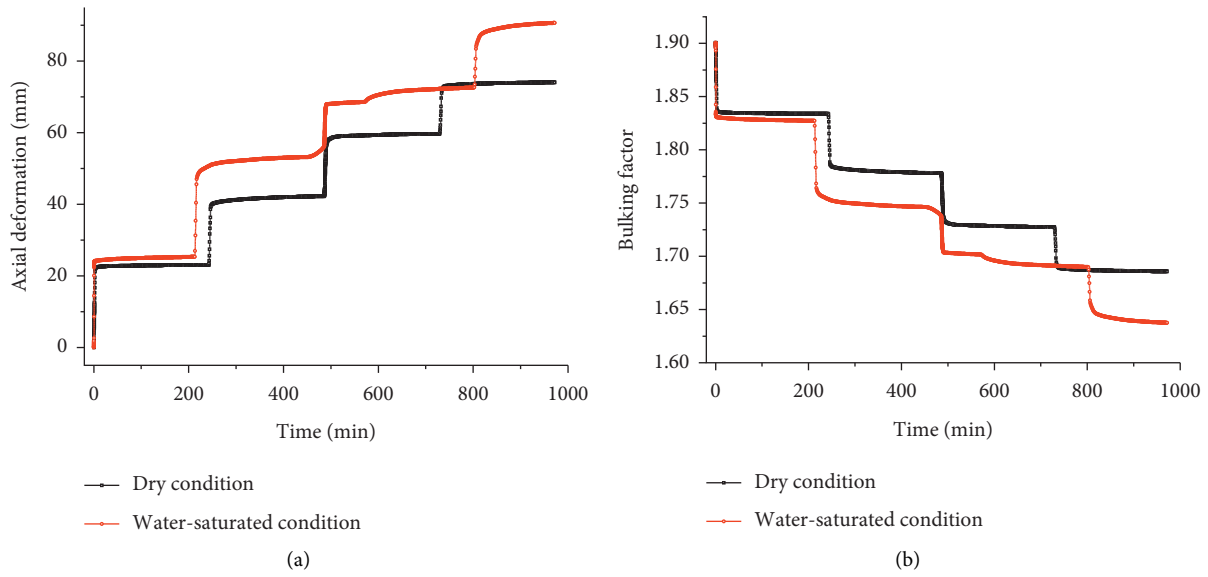

Figure 8: Axial deformation-time curve and bulking factor-time curve of caved gangue specimens. (a) Axial deformation-time curve. (b) Bulking factor-time curve.

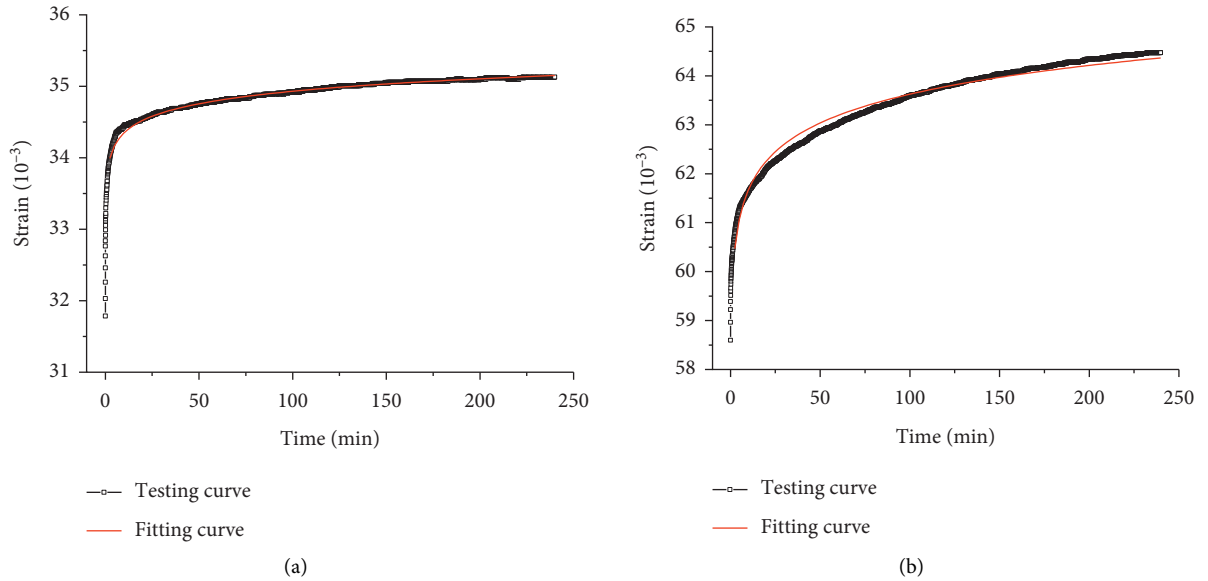

Figure 9: Continued.

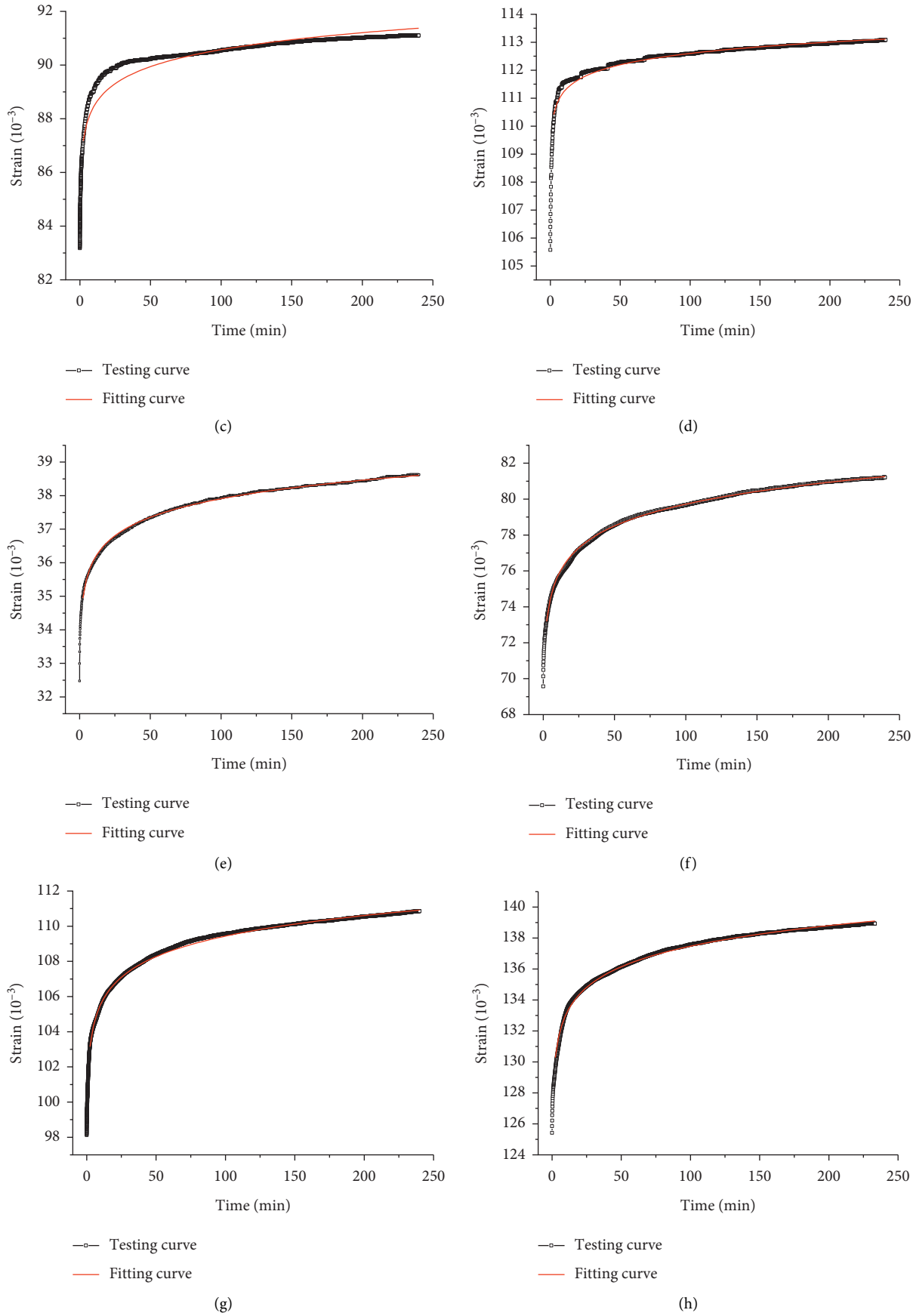

Figure 9: Strain-time curve of caved gangue specimens in constant load stage. (a) 100kN constant load (dry). (b) 200kN constant load (dry). (c) 300kN constant load (dry). (d) 400kN constant load (dry). (e) 100kN constant load (water saturated). (f) 200kN constant load (water -saturated). (g) 300kN constant load (water saturated). (h) 400kN constant load (water saturated).

relationship between strain and time meets the logarithmic relationship. The R-square of each fitting formula is greater than 0.94. In the early stage, the axial strain increases rapidly, then becomes gently. In the late stage, the axial strain is unchanged basically.

The strain D-values of the caved gangue specimens in different stages are shown in Figure 10.

(1) In load stage: From 20 kN to 100 kN, the axial strain D-value is $31.8\times10^{-3}$and 32.5×10^{-3}, respectively, under dry condition and water-saturated condition, which are equal basically and indicate that the water has no effect on the compressive strain of caved gangue specimen. From 100 kN to 200 kN, the axial strain D-value under water-saturated condition is 6.7×10^{-3} greater than that in dry condition, which indicates that the water acting as the lubricant promotes the compressive strain of caved gangue specimen and is conducive to rotation and slipping between each rock block. From 200 kN to 300 kN, the axial strain D-value under dry condition and water-saturated condition is 18.7×10^{-3} and 16.9×10^{-3}, respectively; the latter is less than the former, which is because the previous accumulated strain under water-saturated condition is greater than that under dry condition, and is 81.2×10^{-3} and 64.5×10^{-3}, respectively. From 300 kN to 400 kN, the axial strain D-value is $14.1\times10^{-3}$and 14.0×10^{-3}, respectively, under dry condition and water-saturated condition, which are equal basically.

(2) In constant load stage: In 4 constant load stages, the axial strain D-values under water-saturated condition are all greater than these under dry condition. According to the load from small to large, the increment of the axial strain D-values is 2.8×10^{-3}, 6.5×10^{-3}, 4.8×10^{-3} and 6.2×10^{-3}, which indicates that the water acting as the lubricant promotes the compressive strain of caved gangue specimen and is conducive to rotation and slipping between each rock block. Meanwhile, the water acting as the softening agent reduces the strength of the rock block and is conducive to the crushing of the rock block. The newborn rock blocks may slip and fill the gap between rock blocks, which also promotes the compressive strain of caved gangue specimen. It is worth noting that the crushing of the rock blocks will appear only when the crushing stress is greater than the strength.

3.2. Particle Size Distribution Characteristics. After the testing, the caved gangue specimens under dry condition and water-saturated condition are screened and weighed again. The changes of mass fraction of caved gangue with different particle sizes are shown in Table 3 and Figure 11. Under dry condition and water-saturated condition, the mass fraction of caved gangue with the particle size of 0-5 mm increases by 5.25% and 5.85%, respectively, while the particle size of 5–10 mm increases by 2.46% and 3.09%, respectively. The mass fraction of caved gangue blocks with the particle size of 10–20 mm is basically unchanged, so the particle size of 10–20 mm can be defined as the stable particle size. It does not mean that the load has no effect on the caved gangue blocks with the particle size of 10–20 mm because some caved gangue blocks have obvious new fracture marks after rescreening, which indicates that the mass fraction of caved gangue blocks with the particle size of 10–20 mm is dynamically stabilized, that is, the weight of newborn caved gangue blocks is basically equal to the weight of diminished caved gangue blocks. Under dry condition and water-saturated condition, the mass fraction of caved gangue with the particle size of 20–25 mm decreases by 3.19% and 3.32%, respectively, while the particle size of 25–30 mm decreases by 3.65% and 4.95%, respectively, and the particle size of 30–35 mm decreases by 0.98% and 1.14%, respectively. The mass fraction of caved gangue with the particle size of 35–40 mm is unchanged basically. The particle size distribution of caved gangue specimen provide a strong evidence that many rock blocks are broken into smaller blocks during testing.

3.3. Bearing Deformation Mechanism. During the bearing deformation testing of the caved gangue specimen, there will be a greater frictional force between the inner wall of testing chamber and the caved gangue specimen, which weakens the transfer of axial stress, so the pressure acting on these caved gangue blocks near the bottom of testing chamber is less than that near the top of testing chamber [43]. Because the diameter and height of the caved gangue specimen are 400 mm and 655 mm, respectively, the specimen is narrow and high. The distribution of compressive stress is shown in Figure 12.

The compressive stress of side wall of caved gangue specimen (σ_b) is given by

$$\sigma_b = \frac{\rho g A}{\mu L}\left(1 - \frac{1}{e^{\mu L n' h/A}}\right), \tag{6}$$

where σ_b is the compressive stress of side wall of caved gangue specimen, ρ is the density of caved gangue, g is the gravitational acceleration, μ is the frictional factor between the inner wall of testing chamber and the caved gangue specimen, n' is the specific value of lateral compressive stress and average vertical compressive stress, $n' = \sigma_b/\sigma_{cp}$, σ_{cp} is the average vertical compressive stress, A is the bottom area of caved gangue specimen, L is the perimeter of caved gangue specimen, and h is the height of caved gangue specimen.

The vertical compressive stress of caved gangue specimen (σ) is given by

$$\sigma = \sigma_b\left[1 + 2\mu_0^2 + 2\sqrt{\left(1+\mu_0^2\right)}\left(\mu_0^2 - \mu^2\frac{4x^2}{b^2}\right)\right], \tag{7}$$

where μ_0 is the internal friction coefficient of caved gangue specimen $\mu_0 = \tan\varphi$, φ is the deflection angle of principal

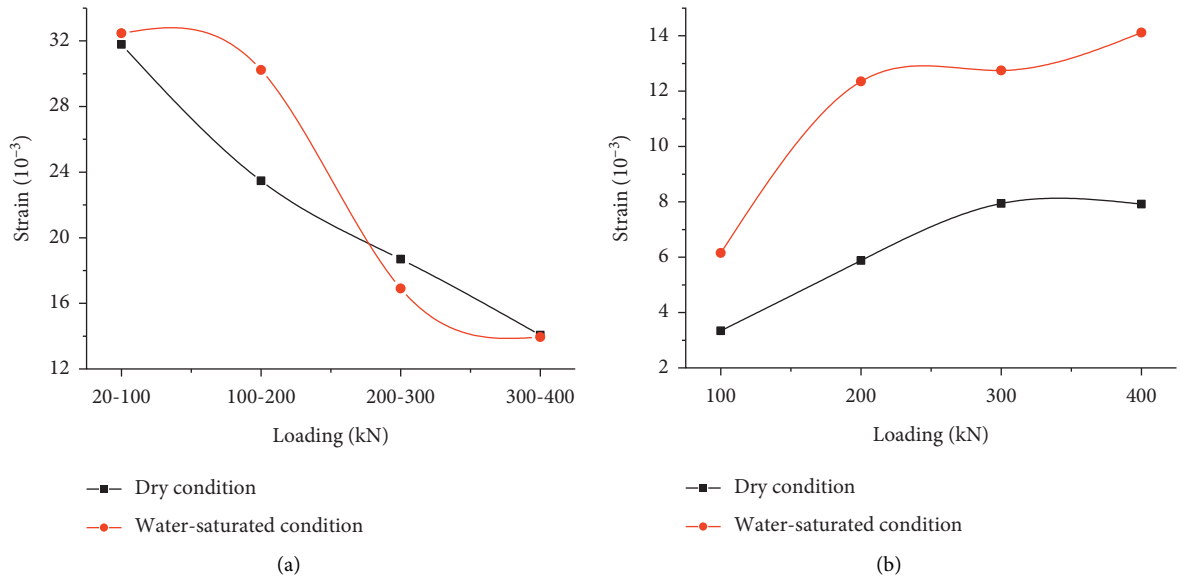

Figure 10: Strain D-values of the caved gangue specimens in different stages. (a) Different load stages. (b) Different constant load stages.

Table 3: Changes of mass fraction of caved gangue with different particle sizes before and after the testing.

Particle size	Mass fraction (%)					
	Dry			Water-saturated		
	Before testing	After testing	D-value	Before testing	After testing	D-value
0–5	0	5.25	5.25	0	5.85	5.85
5–10	5	7.46	2.46	5	8.09	3.09
10–15	10	10.21	0.21	10	10.43	0.43
15–20	20	20.08	0.08	20	20.25	0.25
20–25	30	26.81	-3.19	30	26.68	-3.32
25–30	20	16.35	-3.65	20	15.05	-4.95
30–35	10	9.02	-0.98	10	8.86	-1.14
35–40	5	4.82	-0.18	5	4.78	-0.22

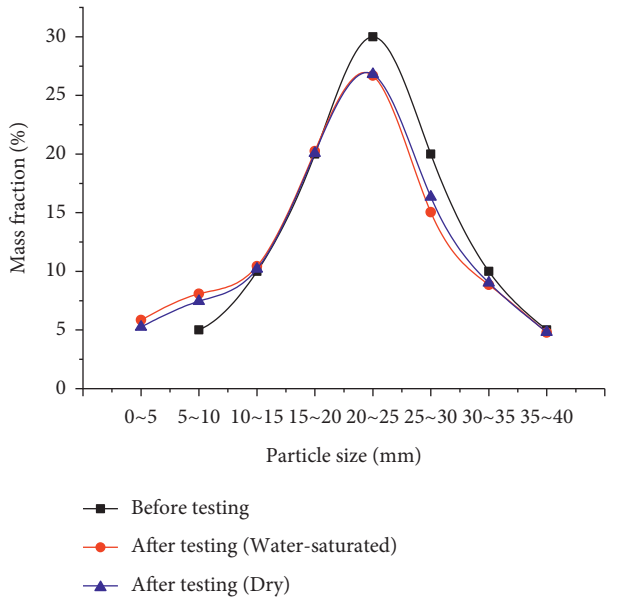

Figure 11: Curves of mass fraction of caved gangue with different particle sizes before and after the testing.

axis in the polar stress diagram near the side surface of caved gangue specimen, b is the diameter of caved gangue specimen, and x is the distance between the calculation point of vertical compressive stress value and the center of caved gangue specimen.

Caved gangue in gob is noncohesive materials and their particles are generally of convex polyhedron shape. The contact between particles can be categorized as angle to face contact and angle to angle contact [44, 45]. A single rock block represented by letter "j" is taken as the object of study, assuming that there are n contacts between rock block "j" and other rock blocks in the caved gangue specimen. Under load, the force and contact area of the ith contact are P_i and δ_i, respectively ($i = 1, 2, \ldots, n$). If there are m contacts on one contact surface labeled "A" of rock block "j", then $m \le n$, as shown in Figure 13.

The normal stress (σ_A) and shear stress (τ_A) acting on the contact surface labeled "A" are given by

$$\sigma_A = \sum_{i=1}^{m} \sigma_i == \sum_{i=1}^{m} \frac{P_i}{\delta_i} \cos\ \alpha_i \tau_A = \sum_{i=1}^{m} \tau_i = \sum_{i=1}^{m} \frac{P_i}{\delta_i} \sin\ \alpha_i, \quad (8)$$

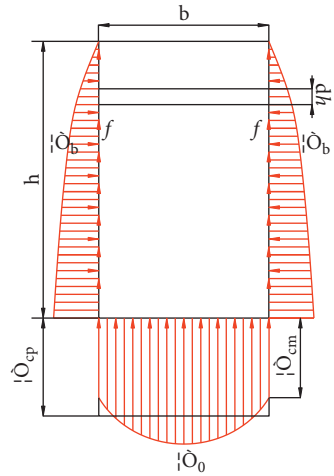

Figure 12: Compressive stress distribution of side wall and bottom of caved gangue specimen.

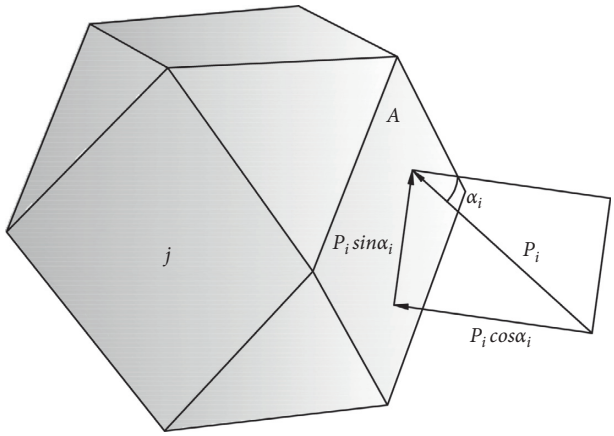

Figure 13: Acting force on the certain contact surface A of rock block j.

where α_i is the angle of intersection of normal of contact surface and acting force.

As a whole, the total normal stress acting on the rock block manifests as compressive stress, which is less than the crushing strength (σ_s) of rock block in the general case; therefore, there will be no crushing between rock blocks. But for some weakness planes, the crushing strength (σ_{sm}) is less than the bearing stress (σ_{im}). Assuming that a total of K weakness planes will be crushed into smaller blocks.

$$\sigma_{im}^k \geq \sigma_{sm}^k \, (k = 1, 2 \ldots K). \tag{9}$$

The total of strain (ε_1) caused by crushing of weakness planes is given by

$$\varepsilon_1 = \sum_{k=1}^{K} \int \left(\sigma_{im}^k - \sigma_{sm}^k\right) \mathrm{d}\zeta_k, \tag{10}$$

where ζ_k is equal to the ratio of strain to crushing stress.

In addition, the shear stress will form the tangential stress (τ_k) on the surface of rock block "j". But because the contact area is very small, the tangential stress is approximated as a uniform distribution. On the kth contact surface, the moment (T_k) about the barycenter of rock block "j" produced by tangential stress is given by

$$T_k = \tau_k \cdot r_k \cdot \delta_k, \tag{11}$$

where r_k is the distance between the kth contact surface and the barycenter of rock block "j".

Around the barycenter of rock block "j", a local coordinate (ξ-η plane) is created, the sum of tangential stress moment vector is given by

$$\begin{aligned} T_{\mathrm{m}\xi} &= \sum_{k=1}^{K} T_k \xi_k = \sum_{k=1}^{K} P_k \sin\, \alpha_k r_k \xi_k \\ T_{\mathrm{m}\eta} &= \sum_{k=1}^{K} T_k \eta_k = \sum_{k=1}^{K} P_k \sin\, \alpha_k r_k \eta_k, \end{aligned} \tag{12}$$

where ξ_k and η_k are the projection coefficients of the local coordinate, which are equal to the ratio of projection value to original value of all shear stress, respectively.

Under the action of moments, the newborn small rock blocks will slide and fill the gap between rock blocks, and the resulting strain (ε_2) is given by

$$\varepsilon_2 = \sum_{k=1}^{K} \int T_k \left(\xi_k \mathrm{d}\theta_\xi^{(k)} + \eta_k \mathrm{d}\theta_\eta^{(k)}\right), \tag{13}$$

where θ_ξ and θ_η are the compliance in shear, which are equal to the ratio of strain to shear stress.

So, during the bearing deformation testing of the caved gangue specimen, the plastic deformation ($_\varepsilon$) is given by

$$\varepsilon = \varepsilon_1 + \varepsilon_2 = \sum_{k=1}^{K} \int \left(\sigma_{im}^k - \sigma_{sm}^k\right) \mathrm{d}\zeta_k + \sum_{k=1}^{K} \int T_k \left(\xi_k \mathrm{d}\theta_\xi^{(k)} + \eta_k \mathrm{d}\theta_\eta^{(k)}\right). \tag{14}$$

It can be seen from the order of magnitude of the strain that ε_2 is greater than ε_1, so the deformation caused by slipping and filling the gap between rock blocks is greater than that caused by the crushing of weakness planes of rock blocks. That is, the major cause of bearing deformation of the caved gangue specimen is that the newborn small rock blocks slip and fill the gap between rock blocks.

The bearing deformation of the caved gangue specimen can be divided into two stages: instantaneous compression deformation and long-term deformation. (1) Instantaneous compression deformation: As the increase of load, the caved gangue specimen becomes compacted gradually. The axial deformation in load stage is more obvious than that in constant load stage, which accounts for 77.8% of total deformation under dry condition, and 67.6% of total deformation under water-saturated condition, the time of load stage is short, the axial deformation will stop basically with the stop of load, but it is inadequate and only relatively stable. The contact between caved gangue blocks is brittle-elastic, the changes of caved gangue blocks mainly include crushing, slipping, and filling, which is more and more prominent with the increase of load. (2) Long-term

deformation: In constant load stage, the impacted crushing of caved gangue is over, but the redistribution of stress between rock blocks will also lead to the crushing of weakness planes of rock blocks, causing the slipping and filling. Under dry condition, the axial deformation in constant load stage accounts for 22.2% of total deformation, and under water-saturated condition, the axial deformation in constant load stage accounts for 32.4% of total deformation. By comparison, the water promotes the compressive strain of caved gangue specimen obviously, especially in constant load stage. The bulk strain of the caved gangue mass is controlled by the rock particle rearrangement, including rotation and slipping between each rock block, and the bulk deformation of a single caved gangue block.

4. Conclusion

(1) The testing system used for bearing deformation testing of caved gangue is developed, which is consisted of load support bracket, load head, testing chamber, servo control system of displacement and load, servo control system of water pressure and water yield, and operating deck. In view of the particle size distribution characteristics and stress state of caved gangue, the size distribution of caved gangue obeys the law of normal distribution, and the load pattern is designed to step load.

(2) With the increase of axial load, the axial deformation of caved gangue increases gradually, the residual bulking coefficient decreases gradually, which are more obvious in load stage than in constant load stage. In the early constant load stage, the axial deformation of caved gangue grows rapidly, then tends to be slow and steady gradually; the relationship between strain and time meets the logarithmic relationship. In load stage, the D-value of axial strain decreases gradually along with the increase of axial load, and in constant load stage, which is opposite.

(3) The bearing deformation of caved gangue is consisted of two parts: instantaneous compression deformation and long-term deformation. For instantaneous compression deformation, the water acting as the lubricant promotes the compressive strain of caved gangue specimen and is conducive to rotation and slipping between each rock block. For long-term deformation, meanwhile, the water acting as the softening agent reduces the strength of the rock block and is conducive to the crushing of the rock block. The newborn rock blocks may slip and fill the gap between rock blocks, which also promotes the compressive strain of caved gangue specimen. The research results have important significance for forecasting and controlling the movement and deformation of overlying strata caused by mining.

Data Availability

The data used to support the findings of this study are included within the article.

Conflicts of Interest

The authors declare that there are no conflicts of interest regarding the publication of this article.

Acknowledgments

This work was supported by the National Science Foundation of China (51704152) and the Natural Science Foundation of Shandong Province (ZR2017BEE001).

References

[1] V. Palchik, "Influence of physical characteristics of weak rock mass on height of caved zone over abandoned subsurface coal mines," *Environmental Geology*, vol. 42, no. 1, pp. 92–101, 2002.

[2] V. Palchik, "Formation of fractured zones in overburden due to longwall mining," *Environmental Geology*, vol. 44, no. 1, pp. 28–38, 2003.

[3] V. Palchik, "Experimental investigation of apertures of mining-induced horizontal fractures," *International Journal of Rock Mechanics and Mining Sciences*, vol. 47, no. 3, pp. 502–508, 2010.

[4] G. Cheng, T. Ma, C. Tang, H. Liu, and S. Wang, "A zoning model for coal mining - induced strata movement based on microseismic monitoring," *International Journal of Rock Mechanics and Mining Sciences*, vol. 94, pp. 123–138, 2017.

[5] D. P. Adhikary and H. Guo, "Modelling of longwall mining-induced strata permeability change," *Rock Mechanics and Rock Engineering*, vol. 48, no. 1, pp. 345–359, 2015.

[6] H. Basarir, I. Ferid Oge, and O. Aydin, "Prediction of the stresses around main and tail gates during top coal caving by 3D numerical analysis," *International Journal of Rock Mechanics and Mining Sciences*, vol. 76, pp. 88–97, 2015.

[7] Q. Wu, J. Shen, W. Liu, and Y. Wang, "A RBFNN-based method for the prediction of the developed height of a water-conductive fractured zone for fully mechanized mining with sublevel caving," *Arabian Journal of Geosciences*, vol. 10, no. 7, pp. 172–180, 2017.

[8] C. Zhang, S. Tu, and Y. Zhao, "Compaction characteristics of the caving zone in a longwall goaf: a review," *Environmental Earth Sciences*, vol. 78, no. 1, pp. 27–42, 2019.

[9] S. Y. Hu, D. D. Han, G. R. Feng et al., "Influence of stress on void ratios of compacted crushed rock masses in coal mine gobs," *Natural Resources Research*, vol. 29, pp. 1362–1373, 2020.

[10] C. Ö. Karacan, "Prediction of porosity and permeability of caved zone in longwall gobs," *Transport in Porous Media*, vol. 82, no. 2, pp. 413–439, 2010.

[11] C. Ö. Karacan and K. Luxbacher, "Stochastic modeling of gob gas venthole production performances in active and completed longwall panels of coal mines," *International Journal of Coal Geology*, vol. 84, no. 2, pp. 125–140, 2010.

[12] M. Li, J. Zhang, N. Zhou, and Y. Huang, "Effect of particle size on the energy evolution of crushed waste rock in coal mines," *Rock Mechanics and Rock Engineering*, vol. 50, no. 5, pp. 1347–1354, 2017.

[13] W. Q. Ma and T. X. Wang, "Experimental study of shear strength features of regenerated rock mass compacted and consolidated by broken soft rocks," *KSCE Journal of Civil Engineering*, vol. 23, pp. 1839–1848, 2019.

[14] J. Chao, M. Yu, T. Chu, X. Han, F. Teng, and P. Li, "Evolution of broken coal permeability under the condition of stress,

temperature, moisture content, and pore pressure," *Rock Mechanics and Rock Engineering*, vol. 52, no. 8, pp. 2803–2814, 2019.

[15] Z. Q. Xiong, X. L. Wang, C. W. Liu, and H. G. Li, "Dynamic development characteristics of caving zone overburden strata in fully-mechanized mining stope under one-pass mining," *Chinese Journal of Rock Mechanics and Engineering*, vol. 33, no. 2, pp. 3692–3698, 2014.

[16] H. P. Xie, H. W. Zhou, J. F. Liu et al., "Mining-induced mechanical behavior in coal seams under different mining layouts," *Journal of China Coal Society*, vol. 36, no. 7, pp. 1067–1074, 2011.

[17] F. Long and S. M. Liu, "A conceptual model to characterize and model compaction behavior and permeability evolution of broken rock mass in coal mine gobs," *International Journal of Coal Geology*, vol. 172, pp. 60–70, 2017.

[18] J. W. Zhang, H. L. Wang, S. J. Chen, and Y. L. Li, "Bearing deformation characteristic of large-size broken rock," *Journal of China Coal Society*, vol. 43, no. 4, pp. 1000–1007, 2018.

[19] H. L. Wang, W. J. Guo, X. Z. Sun, C. Y. Jia, X. Y. Song, and G. B. Zhang, *Disaster Mechanism and Prevention of Water and Sand Inrush across Mining-Induced Roof Fractures*, China Science Publishing and Media Ltd., Beijing, China, 2020.

[20] T. J. Zhang, Y. Guo, M. K. Pang, W. Q. Peng, Y. Li, and S. Zhang, "Creep fractal characteristics of compressed and broken coal rock under different environmental humidity," *Journal of Mining and Safety Engineering*, vol. 37, no. 5, pp. 1037–1044, 2020.

[21] K. Zhang, B. Y. Zhang, J. F. Liu, D. Ma, and H. B. Bai, "Experiment on seepage property and sand inrush criterion for granular rock mass," *Geofluids*, vol. 2017, Article ID 9352618, 10 pages, 2017.

[22] G. B. Zhang, H. L. Wang, S. L. Yan, C. Y. Jia, and X. Y. Song, "Simulated experiment of water-sand inrush across overlying strata fissures caused by mining," *Geofluids*, vol. 2020, Article ID 6614213, 11 pages, 2020.

[23] H. L. Wang, S. J. Chen, and W. J. Guo, "Development and application of test system for water-sand inrush," *Journal of Mining and Safety Engineering*, vol. 36, no. 1, pp. 72–79, 2019.

[24] X. Yang, Y. J. Liu, M. Xue, T. H. Yang, and B. Yang, "Experimental investigation of water-sand mixed fluid initiation and migration in porous skeleton during water and sand inrush," *Geofluids*, vol. 2020, Article ID 8679861, 18 pages, 2020.

[25] B. Yang, T. H. Yang, Z. H. Xu, and X. Yang, "Critical velocity of sand inrush and flow characteristics of water-sand in thick unconsolidated formations of mine in western China," *Journal of Northeastern University*, vol. 39, no. 11, pp. 1648–1652, 2018.

[26] G. Li, Y. Hu, S.-m. Tian, M. weibin, and H.-l. Huang, "Analysis of deformation control mechanism of prestressed anchor on jointed soft rock in large cross-section tunnel," *Bulletin of Engineering Geology and the Environment*, vol. 80, no. 12, pp. 9089–9103, 2021.

[27] M. Gao, J. Xie, Y. Gao et al., "Mechanical behavior of coal under different mining rates: a case study from laboratory experiments to field testing," *International Journal of Mining Science and Technology*, vol. 31, no. 5, pp. 825–841, 2021.

[28] M. Z. Gao, H. C. Hao, S. N. Xue et al., "Discing behavior and mechanism of cores extracted from Songke-2 well at depths below 4,500 m," *International Journal of Rock Mechanics and Mining Sciences*, vol. 149, Article ID 104976, 2022.

[29] C. Zhu, M. Karakus, M. He et al., "Volumetric deformation and damage evolution of Tibet interbedded skarn under multistage constant-amplitude-cyclic loading," *International Journal of Rock Mechanics and Mining Sciences*, vol. 152, Article ID 105066, 2022.

[30] Y.-q. Su, F.-q. Gong, S. Luo, and Z.-x. Liu, "Experimental study on energy storage and dissipation characteristics of granite under two-dimensional compression with constant confining pressure," *Journal of Central South University*, vol. 28, no. 3, pp. 848–865, 2021.

[31] Z.-j. Wu, L.-f. Fan, L. Weng, Q.-s. Liu, and Q. S. Liu, "Micro-failure process and failure mechanism of brittle rock under uniaxial compression using continuous real-time wave velocity measurement," *Journal of Central South University*, vol. 28, no. 2, pp. 556–571, 2021.

[32] Z. Dou, S. X. Tang, X. Y. Zhang et al., "Influence of shear displacement on fluid flow and solute transport in a 3D rough fracture," *Lithosphere*, vol. 2021, Article ID 1569736, 2021.

[33] Z. Dou, Y. M. Liu, X. Y. Zhang et al., "Influence of layer transition zone on rainfall-induced instability of multilayered slope," *Lithosphere*, vol. 2021, Article ID 2277284, 2021.

[34] C. Zhang and L. Zhang, "Permeability characteristics of broken coal and rock under cyclic loading and unloading," *Natural Resources Research*, vol. 28, no. 3, 2019.

[35] Q. Wang, Z. B. Guo, Z. H. Ouyang, S. Y. Yin, and R. Peng, "The influence of crushed rock size on bearing-deformation performance of gangue rib of gob-side entry retaining formed by roof fracturing," *Journal of China University of Mining and Technology*, vol. 51, no. 1, 2022.

[36] B. Y. Yu, S. C. Pan, J. J. Wei, L. Yue, and J. N. Guo, "Particle crushing and permeability evolution of saturated broken rock under compaction," *Journal of Mining and Safety Engineering*, vol. 37, no. 3, pp. 632–638, 2020.

[37] J. Jiang, D. W. Yin, Y. J. Yang, J. B. Ma, and Y. Ge, "Experimental study on long-term load-bearing deformation and fractal characteristics of crushed gangue under dry-wet cycles," *Journal of Mining and Safety Engineering*, vol. 37, no. 1, pp. 176–182, 2020.

[38] Y. J. Xin, H. C. Hao, X. Lü, H. Y. Ji, and D. C. An, "Compaction characteristics test of broken rock in initial lateral pressure," *Journal of China Coal Society*, vol. 43, no. 2, pp. 457–465, 2018.

[39] M. M. Feng, J. Y. Wu, Z. Q. Chen, X. B. Mao, and B. Y. Yu, "Experimental study on the compaction of saturated caved gangue of continuous gradation," *Journal of China Coal Society*, vol. 41, no. 9, pp. 2195–2202, 2016.

[40] C. Zhang, X. C. Zhan, and C. H. Yang, "Mesoscopic simulation of strength and deformation characteristics of coarse grained materials," *Rock and Soil Mechanics*, vol. 34, no. 7, pp. 2077–2083, 2013.

[41] Ministry of Water Resources of the People's Republic of China, *Soecification of Soil Test*, Water Resources and Hydropower Press, Beijing, China, 1999.

[42] W. A. Bishop and D. J. Henkel, *The Measurement of Soils Properties in Triaxial Test*, Edward Arnold, London, UK, 1962.

[43] S. Y. Huang, *Mechanics of Granular Media*, China Machine Press, Beijing, China, 2020.

[44] L. Shao, S. C. Chi, Y. Zhang, and J. Y. Tao, "Study of triaxial shear tests for rockfill based on particle flow code," *Rock and Soil Mechanics*, vol. 34, no. 3, pp. 711–720, 2013.

[45] Y. Huang, J. Li, Y. Teng et al., "Numerical simulation study on macroscopic mechanical behaviors and micro-motion characteristics of gangues under triaxial compression," *Powder Technology*, vol. 320, pp. 668–684, 2017.